Plasma-Catalysis Chemical Looping CH_4 Reforming with water splitting Using Ru/CeO2 nano-catalyst

Rajagopalan V. Ranganathan, Dr. Wang's student, Ruigang Wang, Mruthunjaya Uddi

Abstract: Chemical Looping reactions have the advantage of producing useful chemicals during chemical looping, with minimal energy penalty while achieving Carbon Capture Sequestration (CCS). We present the results of Plasma Catalytic (PC) CH_4 reforming reduction cycle coupled with PC water splitting oxidation cycle to produce hydrogen. We use CH_4+CO_2 flow reduction cycle with nano-powder, Ru/CeO_2. The material is oxidized with H_2O+Ar during the oxidation cycle leading to H_2 production by water splitting. The primary goal is to study the plasma-assisted reforming and water splitting, with the purpose of achieving significant reactions at low temperatures (150-400 ^oC). Significant water splitting H_2 production (76-182 μmole/g total) and CH_4 reforming (43-66 % conversion) was observed in the 150-400 ^oC temperature range, while reactions were observed only at 400 ^oC without plasma, with just the oxygen carrier nano-materials.

1 INTRODUCTION:

The continuous rise of CO_2 emission and its accumulation in the atmosphere is one of the main reasons for global warming. The present atmospheric concentration of CO_2 is already approaching 400 ppm [1]. Therefore, extensive research efforts are under way to decrease CO_2 emission by various means such as Carbon Capture Sequestration (CCS).

Chemical-looping (CL) is a novel and promising technology [2-3] for several applications including oxy-combustion for CCS, H_2 production and CO_2 reuse [4-8]. One of the primary issues in CCS is the energy penalty involved in the removal of CO_2 from the power plant. CL addresses this issue by using a CL material instead of oxygen directly. This makes it easy to separate the CO_2 for CCS. Thus it is economical and energy efficient. Chemical Looping Reforming (CLR) also enables Carbon Capture Utilization (CCU) where CO_2 is utilized to process CH_4 to produce useful products such as CO and H_2.

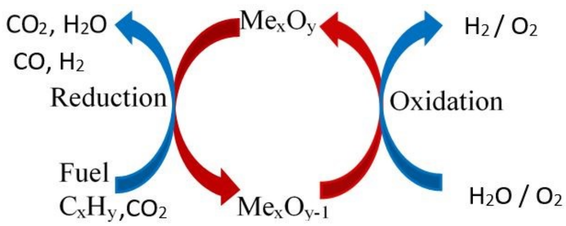

Figure 1. Chemical looping reforming process. (Color lines are seen in online version only).

In Chemical Looping Reforming (CLR) with water splitting, combustion is decomposed into two "redox" steps (**Error! Reference source not found.**) -reduction and oxidation. The redox reactions take place in two separate chambers. Fuel is oxidized by a metal oxide (Me_xO_y) in a fuel reactor to generate CO, H_2, CO_2, and H_2O; during reduction cycle, water vapor is flown over the metal oxide to reoxidize the metal oxide while producing pure H_2. Here, the metal is called the Oxygen Carrier (OC). The OC material can be a metal (ex. Fe, Cu, Ni, Mn, Mg) [9], oxides (CeO_2) or even a perovskite.

There are several CL reactors used both commercially and on lab test scales such as fluidized-bed reactor (FBR) [10-18], moving-bed reactor (MBR) [19-21], a fixed packed-bed reactor (PBR) [22-24], rotating packed-bed reactor (r-PBR) [22-26], rotating cavity solar reactor [27], iron oxide coated honeycombs [28-30], solar reactor for H_2O splitting [31], solar ceria foam reactor for water splitting [32], solar ceria foam reactor for CO_2 splitting [33], disc rotary reactor for water splitting [34], and rotary bed reactor (RBR) [35-36]. Low temperature (<600 °C) operation of RBRs solves most of the issues associated with present reactors and is yet to be tested. However, most OCs have almost no reactivity below 600 °C.

Thermochemical water splitting is a variation of CL to produce H_2 using solar energy, where the reduction of the OC is done by heating the material to high temperatures (~1700 ℃) [27, 32], This involves extreme thermal cycling affecting the reactor lifespan. In isothermal CLRs, a fuel such as syngas or CH_4 is used to reduce the material during the reduction cycle at the same reactor temperature as oxidation cycle. This enables a higher extent of OC reduction and higher amount of H_2 production during the water splitting cycle. However, carbon deposition during the reduction cycling and ways to isolate the different redox gas flows during the redox cycles needs to be considered.

In state of the art isothermal CL experiments with fuel reduction cycle, recently, Zhao et al. [3] studied CL where fuel was used for reducing the OC during the reduction cycle at reactor temperatures below 1000 ℃. They found two orders of magnitude higher production of H_2 (100-300 µmole/g/s) by water splitting compared to thermochemical looping. A review of other materials used for isothermal CL can be found in Zhao et al. [3-4]. It is found that ceria produced more water splitting rates compared to other materials found in the literature.

Some of the most commonly studied OCs are nickel [9, 37-39], copper [9, 40-45], iron [9, 46-48], and manganese-based [9, 40, 49-50] OCs. Expensive noble metals like Pt [51-52], Ru [53-54] show higher catalytic activity and less coke formation in case of dry reforming of methane. One of the options is the nickel-based catalyst, which is reported to improve the reforming of methane [55-57]. Coke formation and agglomeration are primary concerns with Ni-based catalysts.

Recently, plasma-Catalysis (PC) has received much attention due to the possible synergy between nano-catalysts and non-equilibrium low temperature electric plasma discharge. PC has been found to enhance plasma combustion [58-59] and heterogeneous reactions [60-65] at low temperatures. Whitehead et al. [66], demonstrated the experimental PC synergy in the destruction of toluene, considered as an example of atmospheric pollutant, achieving significant energy efficiency over just catalytic or plasma process. They also found an energy saving of ~34 % using the plasma-catalyst combination. Other promising results of PC synergy have been summarized in several reviews [60-65]. The results show endless possibilities when the radicals, ions, electrons, vibrationally, rotationally and electronically excited species produced in a non-equilibrium low temperature plasma is combined with the advantages of nano-catalysts. More recently, Mehta et al. [65] showed the possible advantages of N_2 vibrational excitation in PC synthesis of NH_3 through DFT calculations.

Table 1 shows the various possible synergistic interaction phenomenon between plasma and catalysts [62, 67-68]. The reduction in operation temperature has several advantages in CL reactor design [69] such as lower entropy generation, reduced heat losses, longer reactor lifespan, reduced catalyst deactivation etc. It also opens the opportunities for using low cost solar energy reactors, wind energy, waste heat etc.

Table 1. Plasma catalysis synergy updated from [62, 67-68]

Effects of catalyst on plasma	**Effects of plasma on catalyst**

1) Electric field enhancement 2) Micro-discharge formation in pores 3) Change in discharge type 4) Increased pollutant concentration in plasma (ex. NO_x)	1) Higher adsorption probability at catalyst 2) Higher catalyst surface area 3) Change in catalyst oxidation state 4) Reduction of metal oxide to metallic catalyst 5) Reduced coke formation	6) Change in catalyst work function 7) Hot spot formation 8) Activation by photon irradiation 9) Lowering activation barrier 10) Changing surface reaction pathways

The goal of this study is to achieve CLRs at much lower temperatures (150-500 ^oC) which could enable the development of efficient reactors using waste heat, wind energy or solar energy. We therefore adopt PC to achieve the aforementioned goal using nano-powder 50 : 50 mass ratio of $La_{0.9}Ce_{0.1}NiO_3$ and CeO_2 solid mixture as catalyst with OC combination. The $La_{0.9}Ce_{0.1}NiO_3$ has been found to be a very good CH_4 reforming catalyst [70] while ceria is known for high lattice and surface oxygen ion mobility [71-72] leading to faster reaction rates, lesser carbon deposition. Ceria also has a very good oxygen carrying capacity. Here, we present experimental results of PC- CL reactions with water splitting oxidation cycle, not studied before. A mixture of CH_4 and CO_2 was flown during the reduction cycle corresponding to real oxy-combustion applications. The extent of reduction of the OC is lesser due to the larger partial pressure of O or O_2 in this mixture compared to inert gas flows, such as CH_4 with Ar or He. The oxidation cycle involves H_2O vapor and Ar mixture flow. 100% Ar is used for the purging cycle.

2 EXPERIMENTAL SETUP

2.1 Reactor setup:

The experimental section consists of four parts – a gas delivery system, a central quartz reactor tube, experimental control section, and a flue gas analysis system. The design is based on that of Tianjiao Chen [73], modified for plasma discharge. The system layout and details of the reactor are shown in **Error! Reference source not found.**. The gas delivery system consists of four Brooks GF040 Multiflo thermal mass flow controllers (MFC) which are controlled by a computer interface with an NI card. The NI card is controlled using a home written MATLAB GUI code. Gases such as argon, CH_4, CO_2, O_2 flow through these MFCs. A mixture of CH_4 and CO_2 can be flown during the reduction cycle. Ar is flown during purging and Ar with O_2 or Ar with H_2O during the oxidation cycle. Liquid water can be injected, into the heated Ar flow line, using an automated syringe pump from New Era Pump Systems, which vaporizes as it enters the reactor for the oxidation cycle.

The reactor consists of two concentric quartz tubes, which are placed inside an ATS 3210 split tube furnace. The furnace can heat up to 1100℃ and provide an isothermal environment. The reactive gases are flown into the inner tube first which exit at the open end inside the outer tube, reverse direction and flow out to the exhaust. The inner quartz tube is of ¼" outer diameter (OD) with an expansion section of 3/8" inner diameter (ID) and 2" length. The reactive CL material, dispersed in quartz wool, is placed inside the expansion section of the inner quartz tube. The outside tube is of 1" OD and closed at one end.

A tiny capillary quartz probe (.80 mm OD, 0.53 mm ID) the end of which can be traversed along the inside of the oxygen carrier is used to sample the gases and measure time resolved species at the probe end location. To analyze the gas composition a quadrupole mass spectrometer (QMS), model: MAX300-EGA from Extrel is used. The QMS has a time response of less than 300 ms, 1-250 amu detectability, and a wide bandwidth and concentration detection capability. The QMS is calibrated by flowing known mixture of gases. Signals at m/e=40, 44, 32, 2, 15, 18, 28 are used to measure Ar, CO_2, O_2, H_2, CH_4, H_2O, CO. CO_2 interferes with CO signals at 28 and its signals at 14 and 44 are used to correct the signals at 28 for CO. The QMS calibration showed measurements to be accurate within ± 0.5 %. We were able to flow all the gases (H_2O, CO_2, CO, H_2, CH_4, Ar, O_2) simultaneously for the calibration.

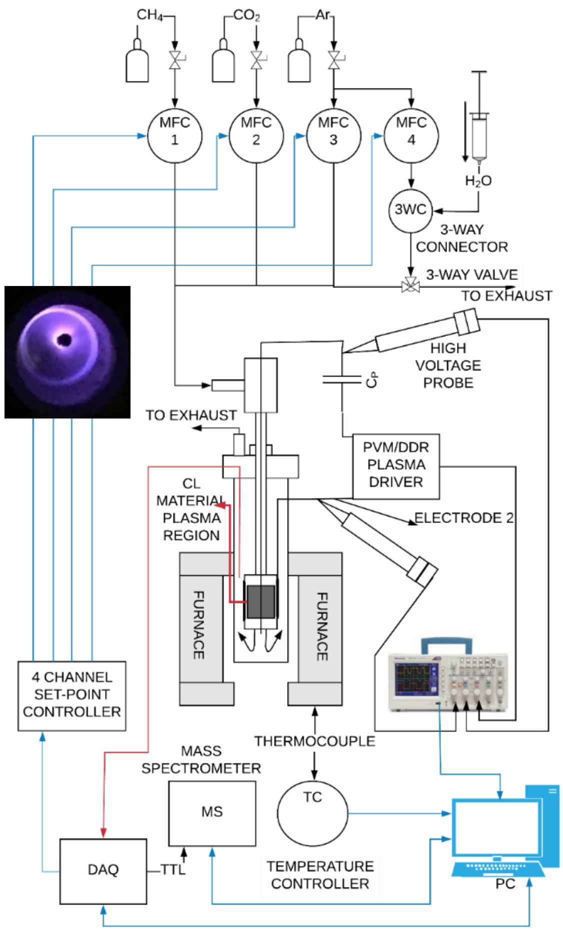

Figure 2. Schematic of the experimental setup (Color lines are seen in the online version only). A bottom view picture of the plasma is shown on the left.

The setup contains two electrodes: one at the center of the inner tube inside a 0.063 ID ceramic tube and the other on the outside of the expansion section of the inner tube, giving rise to Dielectric Barrier Discharge (DBD). One of the electrodes is directly connected to the PVM/DDR plasma driver while the other electrode connected via a 1nF capacitor to the driver. The voltages are measured using two High Voltage Probes (HVPs) connected to the wires connecting the electrode to the plasma driver. The voltages on the HVPs are measured on an oscilloscope and processed to draw Lissajous curves to find the plasma power input by the method explained by Marcin Holub [74].

The measured concentrations of species are plotted as a function of time and used to study the reactions. The materials were characterized using XRD and SEM before and after redox reactions. The total flow rate of gases were maintained at 350 sccm (Standard Cubic Centimeter) during all the redox and purge cycles. The flow during the reduction cycle is a mixture of CH_4 (100 sccm) and CO_2 (250 sccm). Ar is used as purge gas. The flow during the oxidation cycle consists of argon and water vapor (2~10 % H_2O with Ar). All experiments were conducted at 1 atm pressure, and in the temperature range of 150-1000 ºC. For some cases, experiments were done while increasing the temperature (ramp up), and then, while decreasing the temperature (ramp down) of the furnace. This was done to study the effect of high temperature cycling on material structure and reactivity.

2.2 Materials preparation:

The Nickel based Perovskite was prepared in a three step sol-gel [73, 75-76] process. The nitrate salts of the perovskite components are mixed together in the proper ratios with distilled water to create an aqueous solution. Citric acid and Ethylene glycol are also added into the solution. The solution placed on a hotplate and with a magnetic stirrer, until all the water is evaporated. The dry precipitate is then hand ground and calcined for 5 hours in the furnace at a temperature of 300 ℃. The perovskite powder is then removed and hand ground, after which it is calcined for a second cycle at 600 ℃ for 3 hours. After the preparation of the 50 nm Nickel based perovskite powder, it is then combined with 1 micron size ceria powder in a 50:50 mass ratio. This mixture is then sintered at 1000 ℃ for 30 minutes. This mixture is hand ground for 10 min. A total mass of 200 mg was used in all the experiments. SEM images (**Error! Reference source not found.**) showed the size of all particles to be in the range 50-100 nm, before and after redox cycling. The material $La_{0.9}Ce_{0.1}NiO_3 + CeO_2$ (LCN91Ce) is tested in the reactor.

Figure 3. LCN91Ce before (left) and after (right) experiment.

2.3 Calculations

The important parameters used to compare the performance with and without plasma during the reduction cycles are gaseous species conversion, selectivity, and yield. The conversion is the ratio of the total amount of reactant consumed to the total amount of input reactant. The yield of a reaction is defined as the ratio of the desired product produced to the total amount of reactant used. The selectivity is defined as the ratio of desired product produced to the ratio of total reactant consumed. These terms are useful in identifying the consumption of the reactant, formation of the desired product and the selectivity towards a desired product. The following formulas are used for the calculation:

$$\text{CH}_4 \text{ Conversion } (X_{CH_4}) = \left[\frac{\text{Moles of CH}_4 \text{ consumed}}{\text{Moles of CH}_4 \text{ input}}\right] \text{X } 100\ (\%) \tag{1}$$

$$\text{CO}_2 \text{ Conversion } (X_{CO_2}) = \left[\frac{\text{Moles of CO}_2 \text{ consumed}}{\text{Moles of CO}_2 \text{ input}}\right] \text{X } 100\ (\%) \tag{2}$$

$$\text{CO Selectivity } (S_{CO}) = \left[\frac{\text{Moles of CO formed}}{\text{Moles of CH}_4 \text{ consumed} + \text{Moles of CO}_2 \text{ consumed}}\right] \text{X } 100\ (\%) \tag{3}$$

$$\text{H}_2 \text{ Selectivity } (S_{H_2}) = \left[\frac{\text{Moles of H}_2 \text{ formed}}{2 \text{ X Moles of CH}_4 \text{ consumed}}\right] \text{X } 100\ (\%) \tag{4}$$

$$\text{CO Yield } (Y_{CO}) = \left[\frac{\text{Moles of CO formed}}{\text{Moles of CH}_4 \text{ input} + \text{Moles of CO}_2 \text{ input}}\right] \text{X } 100\ (\%) \tag{5}$$

$$\text{H}_2 \text{ Yield } (Y_{H_2}) = \left[\frac{\text{Moles of H}_2 \text{ formed}}{2 \text{ X Moles of CH}_4 \text{ input}}\right] \text{X } 100\ (\%) \tag{6}$$

$$\text{Carbon Balance} = \left[\frac{\begin{array}{c}\text{Sum of Moles of CO, CO}_2 \text{ and CH}_4 \text{ formed(reduction)} \\ +\text{Moles of CO}_2 \text{ formed (oxidation)}\end{array}}{\text{Moles of CH}_4 \text{ input} + \text{Moles of CO}_2 \text{ input}}\right] \text{X } 100\ (\%) \tag{7}$$

3 RESULTS AND DISCUSSIONS

Error! Reference source not found. shows a typical cycle data from the experiment, measured using the Extrel QMS, for one redox cycling at 400 ^{o}C. A single repeated CL cycle consists of a reduction cycle followed by a purge and an oxidation followed by a purge cycle. During the reduction, CH_4 (28.6% by volume) and CO_2 (71.4% by volume) gases are flown. During the purge, an inert gas Ar (100% by volume) is used. For the oxidation cycle, 2~10% H_2O and balance Ar was used. Gases such as CO_2, CH_4, CO, H_2 and H_2O were seen during the reduction cycle. Gases such as H_2 and CO_2 were seen during oxidation cycle. A small spike of CO_2 was observed during the oxidation cycle which increased with temperature. This spike is the result of carbon deposition during the reduction cycle.

Two different sets of experiments were conducted: (1) with CL material and no plasma, and (2) with CL material and plasma. Experiments without plasma were conducted by decreasing the temperature from 400 ^oC to 150 ^oC. The various species such as CO, H_2, CH_4, and CO_2 evolved during the reduction cycle at different temperatures are plotted in **Error! Reference source not found.** and **Error! Reference source not found.**. For the case of CL materials only, reforming was observed at 400 ^oC. For this case, the integrated total number of moles of CO and H_2 produced at 400 ^oC during the reduction cycle were 3303 μmole/g and 547 μmole/g, respectively. At 400 ^oC , the integrated total number of moles of CH_4 and CO_2 were 46131 and 114358 μmole/g. The integrated total number of moles of CH_4 and CO_2 flown was 47369 μmole/g and 118440 μmole/g, respectively, during the reduction cycle. This shows that part of the CO_2 is converted to CO.

With PC experiments, the performance improved significantly in the temperature range of 150 ^oC to 400 ^oC. For this case, the integrated total number of moles of CO and H_2 produced at 400 ^oC during the reduction cycle were 37569 μmole/g and 21312 μmole/g, respectively. The enhancement in case of CO and H_2 is approximately 11 times and 39 times at 400 ^oC.

The higher amount of H_2 by water splitting with PC at all temperatures, is the outcome of greater extent of material reduction due to reactive plasma radicals produced during the reduction cycle such as the CH_x, H, CO by electron impact on CH_4, CO_2. The oxidation of the CL material can be more complete with H_2O vapor in plasma due to abundant O atoms produced by electron impact dissociation of H_2O. It was previously [3] found that water did not completely oxidize ceria (without plasma) and another air flow cycle was required to completely oxidize the ceria at all temperatures.

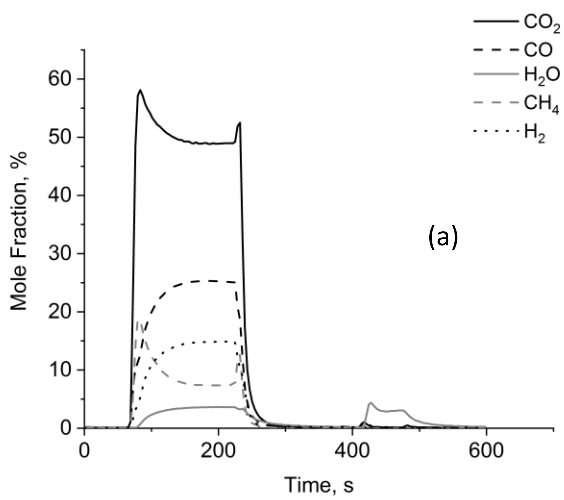

Figure 4. Measured time resolved species mole fraction after flow over the nanomaterial during a reduction/oxidation (redox) cycle, at 1000 °C, 1 atm pressure.

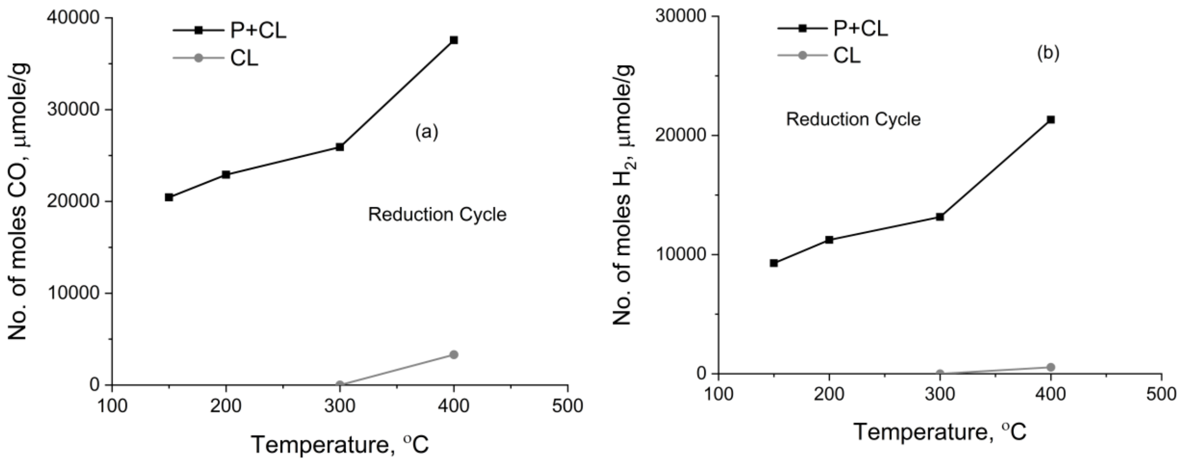

Figure 5. Number of moles of (a) CO and (b) H_2 formed during reduction cycle at various temperatures. P: Plasma.

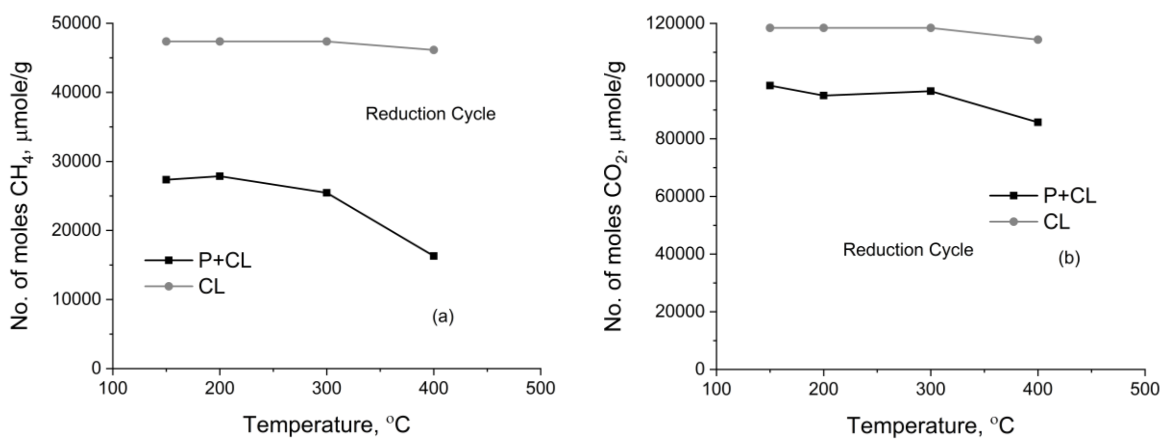

Figure 5. Number of moles of (a) CH_4 and (b) CO_2 consumed during reduction cycle.

The H_2 generated by water splitting during oxidation cycle at different temperatures is plotted in **Error! Reference source not found.**. The experiments without plasma showed hydrogen generation at 400 ^{o}C. With PC, the hydrogen generation was observed at as low as 150 ^{o}C . The hydrogen generated at 400 ^{o}C was close to 182 μmole/g.

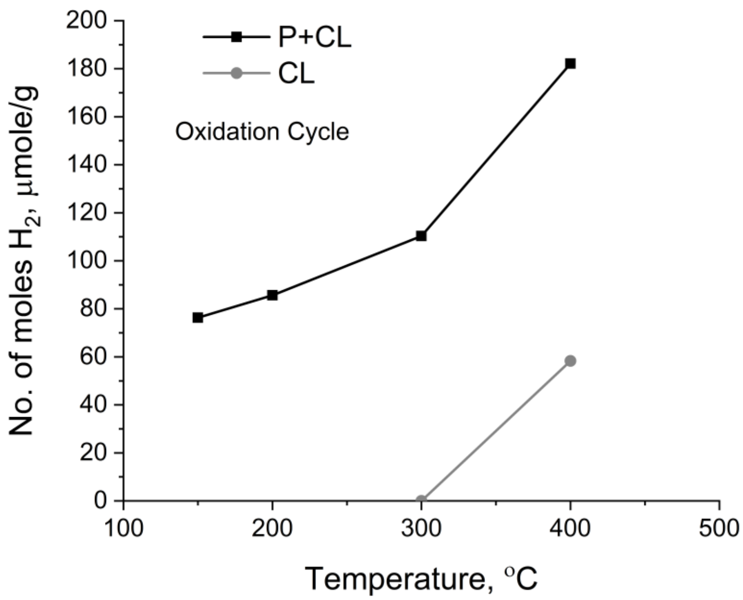

Figure 7. Number of moles of H_2 formed during Oxidation cycle.

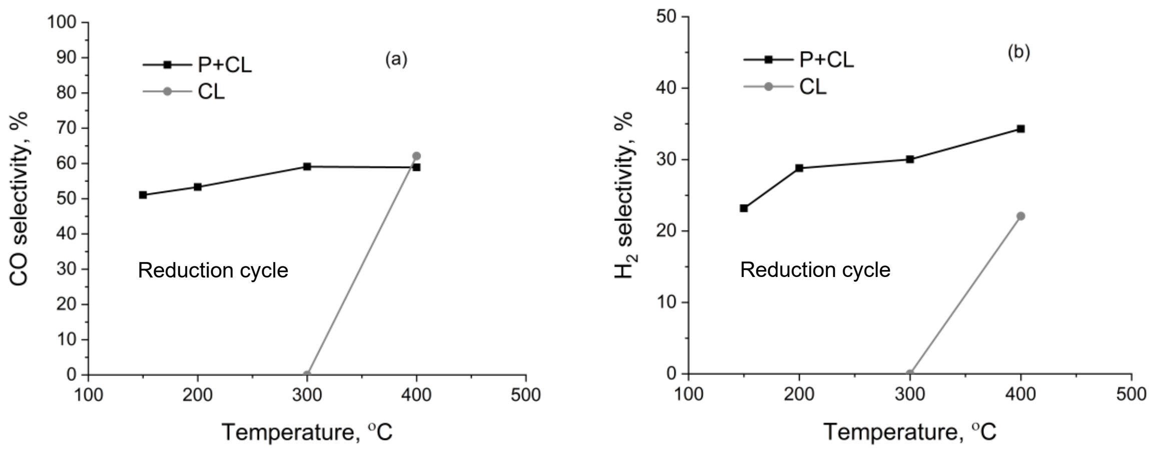

Figure 8. Selectivity (a) CO and (b) H_2 vs. temperature.

The parameters defined in section 2.2 are calculated and plotted in Figure and **Error! Reference source not found.**. Figure 8 shows the selectivity for CO and H_2. For temperatures below 400 °C, the selectivity for CO and H_2 with plasma is better than without plasma. At 400 °C, we see similar selectivity (Figure (a)) to CO while selectivity of H_2 shows a slightly better than without plasma (Figure (b)). Figure 9 shows the percentage of conversion of CH_4 and CO_2 and also the yield of CO and H_2 at different temperatures. For all temperatures 400 °C to 150 °C, the conversions were higher for PC experiments, with CH_4 and CO_2 conversion values of 43.5% and 16.9% respectively at 150 °C. Yabe et al.[77] used Ni/La-ZrO_2, at 150 °C reactor temperature. With 3.7 W of applied power they reported 22.8 % conversion of CH_4 and 24.8 % conversion of CO_2 at an input flow rate of 100 sccm. These values are similar to our CH_4 conversion values of ~18%. Similarly, Plasma-assisted Chemical looping combustion was performed by Zheng et al[78], using a NiO/Fe_2O_3 catalyst at 400 °C. During the reduction cycle, a combination of CH_4 and Ar was used as reducing agent.

During the oxidation cycle, air was used to re-oxidize the material. During the reduction cycle, it enhanced the production of H_2 and during the oxidation cycle, it was used to help in re-oxidation and avoid coking issues. A CH_4 conversion of 39% was achieved using Plasma-assisted chemical looping partial oxidation at 400 ^oC. At 400 ^oC, the current work achieved a CH_4 reforming conversion of ~ 66.9%.

At 400 ^0C yield value for PC with numeric values for the CO and H_2 at 22.6% and 22.4% (**Error! Reference source not found.** (c) and (d)) respectively. In experiments without plasma, CO yield, and H_2 yield were 1.99% and 0.57% at 400 ^oC. Experiments with plasma was able to produce a CO yield of 12 to 15% and an H_2 yield of 9 to 14% from 150 ^oC to 300 ^oC. The comparison among the two cases clearly depicted the following results: with plasma has the highest yield throughout the whole temperature range compared to without plasma experiment (Figure 10 (c) and (d)).

Carbon inflow into the reactor is in the form of CH_4 and CO_2, while carbon outflow is in the form of CH_4, CO, CO_2. The difference between time integrated carbon inflow and carbon outflow for one complete cycle is shown in **Error! Reference source not found.** for different temperatures. Carbon deposition during the reduction cycle is seen as CO_2 emission during the oxidation cycle. This has been accounted for in these carbon balance calculations. For the case of experiments with PC, the carbon deficit gradually increased from 12% at 150 ^oC to ~16% at 400 ^oC. It is possibly because carbon was produced in other forms of C_2 hydrocarbon species such as C_2H_4, C_2H_6 and C_2H_2 which were not measured in the current experiments. These species can be formed in the plasma by the combination of plasma dissociated radicals from CH_4, such as CH_3, CH_2, and CH on the catalyst surface or in the gas phase plasma. These undetected hydrocarbons may have contributed to the carbon balance deficit. Measuring these species and quantifying them will be the focus of future experiments. Oxidative Coupling of Methane (OCM)[79] to form C2 hydrocarbons may have occurred in the initial stages of reduction cycle when the OC is being reduced.

Error! Reference source not found. shows the typical Lissajous curve obtained during the oxidation cycle [76], used to measure plasma input power. In this graph, the discharge voltage is plotted against the capacitor voltage. The power is calculated using a variation of Manley's approach using the formula:

$$P = f.E = f.\oint U_T \frac{dQ}{dt} dt = f.C_P \oint U(t) dU_p \tag{8}$$

Here C_p is an additional capacitor used for measurement whose value is 1nF in our experiments. U(t) is the discharge voltage, Up is the capacitor voltage, f is the frequency of plasma discharge which is 20 kHz. The area in the loops of Figure 11 is proportional to the plasma power supply.

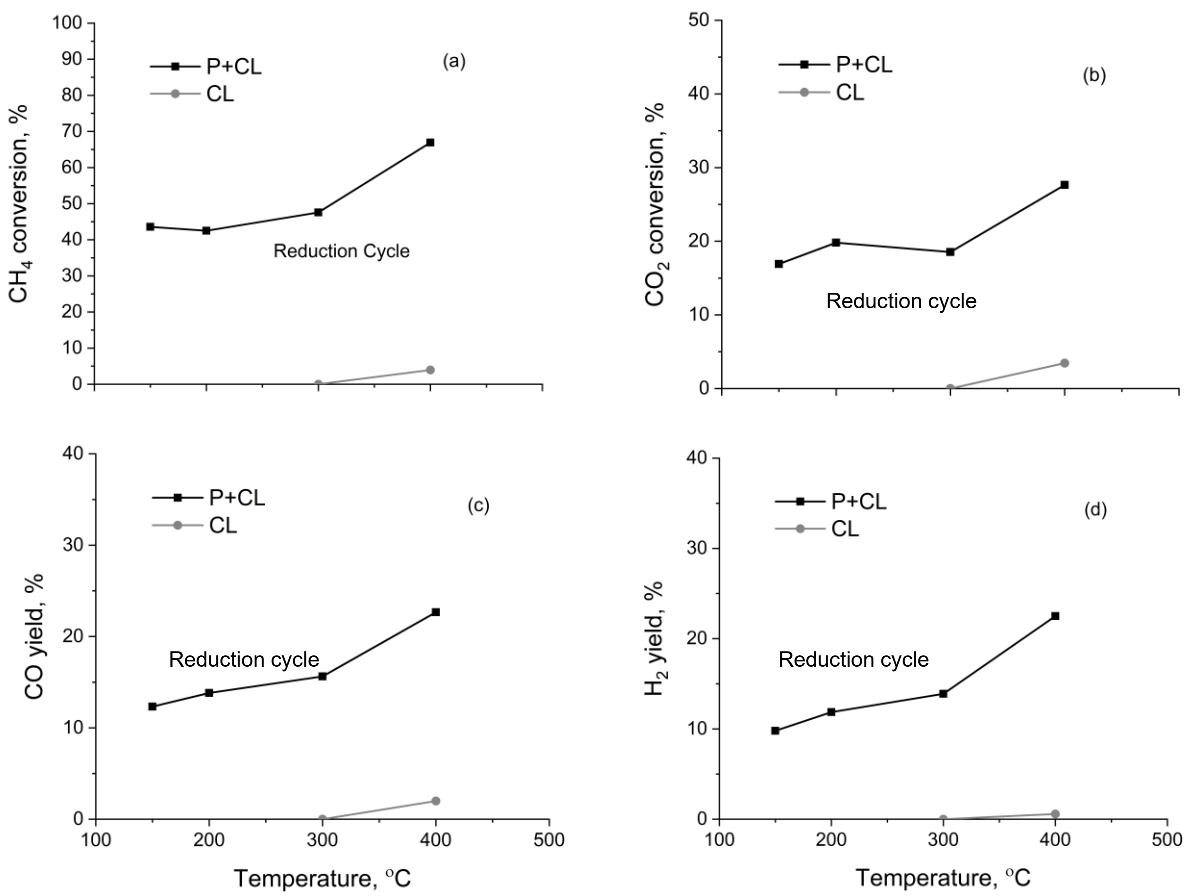

The measured average power during the redox cycles was in the range of 2-6 W for all temperatures. This is much less compared to the furnace heat supply rated at 1.5 kW.

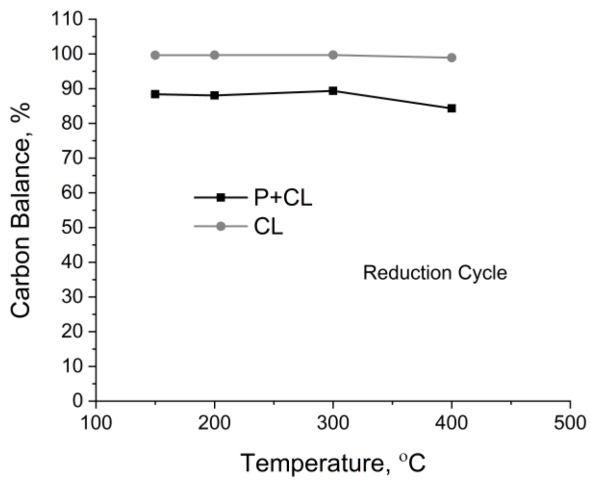

Figure 6. Estimated carbon balance for the experiments at different temperatures.

4 CONCLUSIONS

Plasma-catalysis Ru/CeO_2 was experimented for reforming and water splitting from 150 °C to 400 °C. Experiments were conducted with and without plasma. Without plasma, the redox reactions were observed for temperatures at 400 °C. However, with PC synergy significant reactions and yield were observed in 150-400 °C temperature range. The study showed significant CH_4 and CO_2 conversion at 150 °C. H_2 production by water splitting was observed with PC in 150-400 °C temperature range. PC synergy shows significant efficiency and reactor construction advantages from lab scale to real time applications. For example, the amount of H_2 production through PC water splitting at 150 ^{o}C is approximately more than without plasma at 400 ^{o}C. The required power to run the plasma in this temperature range is only 2-6 W, compared to the maximum furnace power rating of 1.5 kW to get similar results. More efficient surface plasma discharges could be developed for real applications. PC can enhance reactions at lower temperatures efficiently, while maintaining the integrity of materials over long hours.

Acknowledgement:

This material is based upon work supported by the NSF EPSCoR RII-Track-1 Cooperative Agreement OIA-1655280 and the first author was awarded Graduate Research Fellowship NSF EPSCoR. The authors also thank University of Alabama RGC (Research Grants Committee) grants for partial funding of supplies.

5 REFERENCES:

1. International energy agency statistics: 2015.

2. Kvamsdal, H. M.; Jordal, K.; Bolland, O., A quantitative comparison of gas turbine cycles with CO2 capture. *Energy* **2007,** *32* (1), 10-24.

3. Zhao, Z. Redox Kinetics Study for Chemical-looping Combustion and Water Splitting using Nickel and Cerium-based Oxygen Carrier. Dissertation, Massachusetts Institute of Technology, Cambridge, MA, USA, 2016.

4. Zhenlong Zhao; Mruthunjaya Uddi; Nikolai Tsvetkov; Bilge Yildiz; Ghoniem, A. F., Redox Kinetics Study of Fuel Reduced Ceria for Chemical-Looping Water Splitting. *J. of Physical Chemistry C* **2016**.

5. Zhao, Z.; Uddi, M.; Tsvetkov, N.; Yildiz, B.; Ghoniem, A. F., Redox Kinetics Study and Non-Stoichiometry Characterization of Ce0.5Zr0.5O2-δ. *Journal of Physical Chem C* **2016,** *121* (21), 11055-11068

6. Zhao, Z.; Uddi, M.; Tsvetkov, N.; Yildiz, B.; Ghoniem, A. F., Enhanced intermediate-temperature CO2 splitting using nonstoichiometric ceria and ceria-zirconia. *Physical Chemistry Chemical Physics* **2017,** *19* (37), 25774-25785.

7. Zhao, Z.; Uddi, M.; Tsvetkov, N.; Yildiz, B.; Ghoniem, A. F., Redox Kinetics and Nonstoichiometry of Ce0.5Zr0.5O2−δ for Water Splitting and Hydrogen Production. *The Journal of Physical Chemistry C* **2017,** *121* (21), 11055-11068.

8. Zhao Z, U. M., Chen T, Ghoniem A F, Oxidation Study for Chemical-looping Combustion Using Thin Nickel Foils. In *9th U. S. National Combustion Meeting*, Cincinnati, Ohio, 2015.

9. Adánez, J.; de Diego, L. F.; García-Labiano, F.; Gayán, P.; Abad, A.; Palacios, J. M., Selection of Oxygen Carriers for Chemical-Looping Combustion. *Energy & Fuels* **2004,** *18* (2), 371-377.

10. Adanez, J.; Abad, A.; Garcia-Labiano, F.; Gayan, P.; Luis, F., Progress in chemical-looping combustion and reforming technologies. *Progress in Energy and Combustion Science* **2012,** *38* (2), 215-282.

11. Linderholm, C.; Mattisson, T.; Lyngfelt, A., Long-term integrity testing of spray-dried particles in a 10-kW chemical-looping combustor using natural gas as fuel. *Fuel* **2009,** *88* (11), 2083-2096.

12. Adánez, J.; Gayán, P.; Celaya, J.; de Diego, L. F.; García-Labiano, F.; Abad, A., Chemical Looping Combustion in a 10 kWth Prototype Using a CuO/Al2O3 Oxygen Carrier: Effect of Operating Conditions on Methane Combustion. *Industrial & Engineering Chemistry Research* **2006,** *45* (17), 6075-6080.

13. Abad, A.; Mattisson, T.; Lyngfelt, A.; Rydén, M., Chemical-looping combustion in a 300 W continuously operating reactor system using a manganese-based oxygen carrier. *Fuel* **2006,** *85* (9), 1174-1185.

14. Pröll, T.; Kolbitsch, P.; Bolhàr-Nordenkampf, J.; Hofbauer, H., A novel dual circulating fluidized bed system for chemical looping processes. *AIChE Journal* **2009,** *55* (12), 3255-3266.

15. Berguerand, N.; Lyngfelt, A., Chemical-Looping Combustion of Petroleum Coke Using Ilmenite in a 10 kWth Unit−High-Temperature Operation. *Energy & Fuels* **2009,** *23* (10), 5257-5268.

16. Shen, L.; Wu, J.; Xiao, J.; Song, Q.; Xiao, R., Chemical-Looping Combustion of Biomass in a 10 kWth Reactor with Iron Oxide As an Oxygen Carrier. *Energy & Fuels* **2009,** *23* (5), 2498-2505.

17. Gu, H.; Shen, L.; Xiao, J.; Zhang, S.; Song, T., Chemical Looping Combustion of Biomass/Coal with Natural Iron Ore as Oxygen Carrier in a Continuous Reactor. *Energy & Fuels* **2011,** *25* (1), 446-455.

18. D. Kunii, O. L., *Fluidization Engineering*. 2nd Edition ed.; Butterworth-Heinemann: Boston, Massachusetts, 1991.

19. Fan, L. S., *Chemical looping systems for fossil energy conversions*. John Wiley & Sons, Inc.: Hoboken, New Jersey, 2010.

20. Li, F.; Zeng, L.; Velazquez-Vargas, L. G.; Yoscovits, Z.; Fan, L.-S., Syngas chemical looping gasification process: Bench-scale studies and reactor simulations. *AIChE Journal* **2010,** *56* (8), 2186-2199.

21. Li, F.; Zeng, L.; Fan, L.-S., Biomass direct chemical looping process: Process simulation. *Fuel* **2010,** *89* (12), 3773-3784.

22. Noorman, S.; van Sint Annaland, M.; Kuipers, Packed Bed Reactor Technology for Chemical-Looping Combustion. *Industrial & Engineering Chemistry Research* **2007,** *46* (12), 4212-4220.

23. Noorman, S.; van Sint Annaland, M.; Kuipers, J. A. M., Experimental validation of packed bed chemical-looping combustion. *Chemical Engineering Science* **2010,** *65* (1), 92-97.

24. Noorman, S.; Gallucci, F.; van Sint Annaland, M.; Kuipers, J. A. M., Experimental Investigation of Chemical-Looping Combustion in Packed Beds: A Parametric Study. *Industrial & Engineering Chemistry Research* **2011,** *50* (4), 1968-1980.

25. Dahl, I. M.; Bakken, E.; Larring, Y.; Spjelkavik, A. I.; Håkonsen, S. F.; Blom, R., On the development of novel reactor concepts for chemical looping combustion. *Energy Procedia* **2009,** *1* (1), 1513-1519.

26. Håkonsen, S. F.; Blom, R., Chemical Looping Combustion in a Rotating Bed Reactor – Finding Optimal Process Conditions for Prototype Reactor. *Environmental Science & Technology* **2011,** *45* (22), 9619-9626.

27. Steinfeld, A., Solar thermochemical production of hydrogen—a review. *Solar Energy* **2005,** *78* (5), 603-615.

28. Neises, M., Roeb, M., Schmücker, M., Sattler, C. and Pitz-Paal, R., Kinetic investigations of the hydrogen production step of a thermochemical cycle using mixed iron oxides coated on ceramic substrates. *Int. J. Energy Res.* **2010,** *34*, 651–661.

29. Roeb, M.; Säck, J. P.; Rietbrock, P.; Prahl, C.; Schreiber, H.; Neises, M.; de Oliveira, L.; Graf, D.; Ebert, M.; Reinalter, W.; Meyer-Grünefeldt, M.; Sattler, C.; Lopez, A.; Vidal, A.; Elsberg, A.; Stobbe, P.; Jones, D.; Steele, A.; Lorentzou, S.; Pagkoura, C.; Zygogianni, A.; Agrafiotis, C.; Konstandopoulos, A. G., Test operation of a 100 kW pilot plant for solar hydrogen production from water on a solar tower. *Solar Energy* **2011,** *85* (4), 634-644.

30. Roeb, M. N., Martina; Monnerie, Nathalie; Call, Friedemann; Simon, Heike; Sattler, Christian; Schmücker, Martin; Pitz-Paal, Robert; , Materials-Related Aspects of Thermochemical Water and Carbon Dioxide Splitting: A Review. *Materials* **2012,** *5* (11), 2015.

31. Kodama, T., High-temperature solar chemistry for converting solar heat to chemical fuels. *Progress in Energy and Combustion Science* **2003,** *29* (6), 567-597.

32. Chueh, W. C.; Falter, C.; Abbott, M.; Scipio, D.; Furler, P.; Haile, S. M.; Steinfeld, A., High-Flux Solar-Driven Thermochemical Dissociation of CO2 and H2O Using Nonstoichiometric Ceria. *Science* **2010,** *330* (6012), 1797-1801.

33. Furler, P.; Scheffe, J.; Gorbar, M.; Moes, L.; Vogt, U.; Steinfeld, A., Solar Thermochemical CO2 Splitting Utilizing a Reticulated Porous Ceria Redox System. *Energy & Fuels* **2012,** *26* (11), 7051-7059.

34. Kaneko, H.; Miura, T.; Fuse, A.; Ishihara, H.; Taku, S.; Fukuzumi, H.; Naganuma, Y.; Tamaura, Y., Rotary-Type Solar Reactor for Solar Hydrogen Production with Two-step Water Splitting Process. *Energy & Fuels* **2007,** *21* (4), 2287-2293.

35. Zhao Zhenlong; Chen Tianjiao; F, G. A., Design of a rotary reactor for chemical-looping combustion. Part 1: Fundamentals and design methodology. **2014,** *121*, 327–343.

36. Zhao Z, C. T., Ghoniem A F, Design of a rotary reactor for chemical-looping combustion. Part 2: Comparison of copper-, nickel-, and iron-based oxygen carriers. **2014,** *121*, 344–360.

37. Mattisson, T.; Johansson, M.; Lyngfelt, A., The use of NiO as an oxygen carrier in chemical-looping combustion. *Fuel* **2006,** *85* (5), 736-747.

38. Johansson, M.; Mattisson, T.; Lyngfelt, A.; Abad, A., Using continuous and pulse experiments to compare two promising nickel-based oxygen carriers for use in chemical-looping technologies. *Fuel* **2008,** *87* (6), 988-1001.

39. Gayán, P.; de Diego, L.; García-Labiano, F.; Adánez, J.; Abad, A.; Dueso, C., *Effect of support on reactivity and selectivity of Ni-based oxygen carriers for chemical-looping combustion*. 2012; Vol. 87, p 2641-2650.

40. Cho, P.; Mattisson, T.; Lyngfelt, A., Comparison of iron-, nickel-, copper- and manganese-based oxygen carriers for chemical-looping combustion. *Fuel* **2004,** *83* (9), 1215-1225.

41. de Diego, L. F.; García-Labiano, F.; Adánez, J.; Gayán, P.; Abad, A.; Corbella, B. M.; María Palacios, J., Development of Cu-based oxygen carriers for chemical-looping combustion. *Fuel* **2004,** *83* (13), 1749-1757.

42. Gayán, P.; Adánez-Rubio, I.; Abad, A.; de Diego, L. F.; García-Labiano, F.; Adánez, J., Development of Cu-based oxygen carriers for Chemical-Looping with Oxygen Uncoupling (CLOU) process. *Fuel* **2012,** *96* (Supplement C), 226-238.

43. Corbella, B. M.; De Diego, L.; García, F.; Adánez, J.; Palacios, J. M., The Performance in a Fixed Bed Reactor of Copper-Based Oxides on Titania as Oxygen Carriers for Chemical Looping Combustion of Methane. *Energy & Fuels* **2005,** *19* (2), 433-441.

44. García-Labiano, F.; Adánez, J.; de Diego, L. F.; Gayán, P.; Abad, A., Effect of Pressure on the Behavior of Copper-, Iron-, and Nickel-Based Oxygen Carriers for Chemical-Looping Combustion. *Energy & Fuels* **2006,** *20* (1), 26-33.

45. Chuang, S. Y.; Dennis, J. S.; Hayhurst, A. N.; Scott, S. A., Development and performance of Cu-based oxygen carriers for chemical-looping combustion. *Combustion and Flame* **2008,** *154* (1), 109-121.

46. Johansson, M.; Mattisson, T.; Lyngfelt, A., Investigation of Fe2O3 with MgAl2O4 for chemical-looping combustion. *Industrial & engineering chemistry research* **2004,** *43* (22), 6978-6987.

47. Mattisson, T.; Johansson, M.; Lyngfelt, A., Multicycle Reduction and Oxidation of Different Types of Iron Oxide ParticlesApplication to Chemical-Looping Combustion. *Energy & Fuels* **2004,** *18* (3), 628-637.

48. Rydén, M.; Cleverstam, E.; Johansson, M.; Lyngfelt, A.; Mattisson, T., Fe2O3 on Ce-, Ca-, or Mg-stabilized ZrO2 as oxygen carrier for chemical-looping combustion using NiO as additive. *AIChE Journal* **2010,** *56* (8), 2211-2220.

49. Mattisson, T.; Järdnäs, A.; Lyngfelt, A., Reactivity of Some Metal Oxides Supported on Alumina with Alternating Methane and OxygenApplication for Chemical-Looping Combustion. *Energy & Fuels* **2003,** *17* (3), 643-651.

50. Johansson, M.; Mattisson, T.; Lyngfelt, A., Investigation of Mn₃O₄ With Stabilized ZrO₂ for Chemical-Looping Combustion. *Chemical Engineering Research and Design 84* (9), 807-818.

51. Sadykov, V. A.; Gubanova, E. L.; Sazonova, N. N.; Pokrovskaya, S. A.; Chumakova, N. A.; Mezentseva, N. V.; Bobin, A. S.; Gulyaev, R. V.; Ishchenko, A. V.; Krieger, T. A.; Mirodatos, C., Dry reforming of methane over Pt/PrCeZrO catalyst: Kinetic and mechanistic features by transient studies and their modeling. *Catalysis Today* **2011,** *171* (1), 140-149.

52. Stagg-Williams, S. M.; Noronha, F. B.; Fendley, G.; Resasco, D. E., CO2 Reforming of CH4 over Pt/ZrO2 Catalysts Promoted with La and Ce Oxides. *Journal of Catalysis* **2000,** *194* (2), 240-249.

53. Chen, J.; Yao, C.; Zhao, Y.; Jia, P., Synthesis gas production from dry reforming of methane over Ce0.75Zr0.25O2-supported Ru catalysts. *International Journal of Hydrogen Energy* **2010,** *35* (4), 1630-1642.

54. Whang, H. S.; Choi, M. S.; Lim, J.; Kim, C.; Heo, I.; Chang, T.-S.; Lee, H., Enhanced activity and durability of Ru catalyst dispersed on zirconia for dry reforming of methane. *Catalysis Today* **2017,** *293* (Supplement C), 122-128.

55. Abdullah, B.; Ghani, N. A. A.; Vo, D.-V. N., Recent Advances in Dry Reforming of Methane over Ni-based Catalysts. *Journal of Cleaner Production* **2017**.

56. Huang, L.; Zhang, F.; Wang, N.; Chen, R.; Hsu, A. T., Nickel-based perovskite catalysts with iron-doping via self-combustion for hydrogen production in auto-thermal reforming of Ethanol. *International Journal of Hydrogen Energy* **2012,** *37* (2), 1272-1279.

57. Hayakawa, T.; Suzuki, S.; Nakamura, J.; Uchijima, T.; Hamakawa, S.; Suzuki, K.; Shishido, T.; Takehira, K., CO2 reforming of CH4 over Ni/perovskite catalysts prepared by solid phase crystallization method. *Applied Catalysis A: General* **1999,** *183* (2), 273-285.

58. Ju, Y.; Lefkowitz, J. K.; Reuter, C. B.; Won, S. H.; Yang, X.; Yang, S.; Sun, W.; Jiang, Z.; Chen, Q., Plasma Assisted Low Temperature Combustion. *Plasma Chemistry and Plasma Processing* **2016,** *36* (1), 85-105.

59. M Uddi; N Jiang; E Mintuossov; and, I. V. A.; Lempert, W., Atomic Oxygen Measurements in Air and Air/Fuel Nanosecond Pulse Discharges by Two Photon Laser Induced Fluorescence. *Proceedings of the Combustion Institute* **2009,** *32*, 929- 936.

60. Hyun-Ha, K., Nonthermal Plasma Processing for Air-Pollution Control: A Historical Review, Current Issues, and Future Prospects. *Plasma Processes and Polymers* **2004,** *1* (2), 91-110.

61. Kim;, H.-H.; Teramoto;, Y.; Ogata;, A.; Takagi;, H.; Nanba, T., Plasma Catalysis for Environmental Treatment and Energy Applications. *Plasma Chem Plasma Process* **2016,** *36* (45).

62. Neyts, E. C.; Bogaerts, A., Understanding plasma catalysis through modelling and simulation—a review. *Journal of Physics D: Applied Physics* **2014,** *47* (22), 224010.

63. Kim, T.; Jo, S.; Song, Y.-H.; Lee, D. H., Synergetic mechanism of methanol–steam reforming reaction in a catalytic reactor with electric discharges. *Applied Energy* **2014,** *113*, 1692-1699.

64. Whitehead, J. C., Plasma–catalysis: the known knowns, the known unknowns and the unknown unknowns. *Journal of Physics D: Applied Physics* **2016,** *49* (24), 243001.

65. Mehta, P.; Barboun, P.; Herrera, F. A.; Kim, J.; Rumbach, P.; Go, D. B.; Hicks, J. C.; Schneider, W. F., Overcoming ammonia synthesis scaling relations with plasma-enabled catalysis. *Nature Catalysis* **2018,** *1* (4), 269-275.

66. Whitehead, J. C., Plasma catalysis: A solution for environmental problems. In *Pure and Applied Chemistry*, 2010; Vol. 82, p 1329.

67. Janev, R. K.; Reiter, D., Collision processes of CHy and CHy+ hydrocarbons with plasma electrons and protons. *Physics of Plasmas* **2002,** *9* (9), 4071-4081.

68. Kim, H.-H.; Ogata, A.; Futamura, S., Oxygen partial pressure-dependent behavior of various catalysts for the total oxidation of VOCs using cycled system of adsorption and oxygen plasma. *Applied Catalysis B: Environmental* **2008,** *79* (4), 356-367.

69. Motzfeldt, K., *High Temperature Experiments in Chemistry and Materials Science*. John Wiley& Sons, Ltd.: 2013.

70. Gallego, G. S.; Marín, J. G.; Batiot-Dupeyrat, C.; Barrault, J.; Mondragón, F., Influence of Pr and Ce in dry methane reforming catalysts produced from La1−xAxNiO3−δ perovskites. *Applied Catalysis A: General* **2009,** *369* (1), 97-103.

71. Wang, R.; Crozier, P. A.; Sharma, R., Structural Transformation in Ceria Nanoparticles during Redox Processes. *The Journal of Physical Chemistry C* **2009,** *113* (14), 5700-5704.

72. Li, J.; Liu, Z.; Wang, R., Support structure and reduction treatment effects on CO oxidation of SiO_2 nanospheres and CeO_2 nanorods supported ruthenium catalysts. *Journal of Colloid and Interface Science* **2018,** *531*, 204-215.

73. Chen, T. Experimental Characterization and Chemical Kinetic Study of Chemical Looping Combustion. MIT, Cambridge, 2013.

74. Holub, M., On the measurement of plasma power in atmospheric pressure DBD plasma reactors. *International Journal of Applied Electromagnetics and Mechanics* **2012,** *39*, 81 - 87.

75. Dave, B. C.; Lockwood, S. B., Sol-Gel Method. In *Encyclopedia of Nanotechnology*, Bhushan, B., Ed. Springer Netherlands: Dordrecht, 2012; pp 2459-2470.

76. Mahendraprabhu, K.; Elumalai, P., Influence of citric acid on formation of Ni/NiO nanocomposite by sol–gel synthesis. *Journal of Sol-Gel Science and Technology* **2015,** *73* (2), 428-433.

77. Yabe, T.; Mitarai, K.; Oshima, K.; Ogo, S.; Sekine, Y., Low-temperature dry reforming of methane to produce syngas in an electric field over La-doped Ni/ZrO_2 catalysts. *Fuel Processing Technology* **2017,** *158*, 96-103.

78. Zheng, Y.; Grant, R.; Hu, W.; Marek, E.; Scott, S. A., H_2 production from partial oxidation of CH_4 by Fe_2O_3-supported Ni-based catalysts in a plasma-assisted packed bed reactor. *Proceedings of the Combustion Institute* **2018**.

79. Sugiura, K.; Ogo, S.; Iwasaki, K.; Yabe, T.; Sekine, Y., Low-temperature catalytic oxidative coupling of methane in an electric field over a Ce–W–O catalyst system. *Scientific Reports* **2016,** *6*, 25154.